EDGE ARTICLE

Check for updates

Sequential electron transfer governs the UV-induced self-repair of DNA photolesions†

Rafał Szabla, [ID] *[ab] Holger Kruse, [ID] [b] Petr Stadlbauer,[bc] Jiří Šponer [ID] [b] and Andrzej L. Sobolewski[a]

Cyclobutane pyrimidine dimers (CpDs) are among the most common DNA lesions occurring due to the interaction with ultraviolet light. While photolyases have been well known as external factors repairing CpDs, the intrinsic self-repairing capabilities of the GAT=T DNA sequence were discovered only recently and are still largely obscure. Here, we elucidate the mechanistic details of this self-repair process by means of MD simulations and QM/MM computations involving the algebraic diagrammatic construction to the second order [ADC(2)] method. We show that local UV-excitation of guanine may be followed by up to three subsequent electron transfers, which may eventually enable efficient CpD ring opening when the negative charge resides on the T=T dimer. Consequently, the molecular mechanism of GAT=T self-repair can be envisaged as sequential electron transfer (SET) occurring downhill along the slope of the S_1 potential energy surface. Even though the general features of the SET mechanism are retained in both of the studied stacked conformers, our optimizations of different S_1/S_0 state crossings revealed minor differences which could influence their self-repair efficiencies. We expect that such assessment of the availability and efficiency of the SET process in other DNA oligomers could hint towards other sequences exhibiting similar photochemical properties. Such explorations will be particularly fascinating in the context of the origins of biomolecules on Earth, owing to the lack of external repairing factors in the Archean age.

Introduction

Dimerization of DNA bases is one of the most detrimental phenomena occurring during the exposure of nucleic acid strands to UV-light.[1] Cyclobutane pyrimidine dimers (CpDs) and (6-4) lesions can be classified among the most frequent photodimers and are responsible for mutagenic processes driven by hindered transcription and DNA replication.[2] To protect living organisms from such UV-activated stress, nature developed sophisticated enzymes, *i.e.* photolyases, which selectively repair CpDs and (6-4) lesions *via* electron transfer or proton-coupled electron transfer processes.[3,4] Despite the existence of repairing machinery, DNA photolesions are a common cause of skin cancer[1,5–7] and the mechanistic details of their

formation and repair have been attracting significant attention involving both experimental and theoretical studies.[8–17]

The vulnerability of DNA and RNA to the harmful effects of UV-radiation is particularly intriguing in the context of the origins of life. First of all, it is reasonable to assume that the highly sophisticated photolyases were absent during the emergence of the first oligonucleotides. Furthermore, recent theoretical estimates showed that much higher amounts of UV-light were reaching the surface of the Archean Earth, owing to the lack of oxygen in the atmosphere and higher Sun activity in the ultraviolet spectral range.[18–22] Interestingly, a recent work by Bucher *et al.*[23] revealed that specific DNA sequences may promote very efficient self-repair driven by photoinduced electron transfer to the CpD lesion containing two dimerized thymine bases (T=T). This remarkable property was discovered for the GAT=T sequence in single and double strands, while no repair was reported for the TAT=T and AT=T oligomers.[23] The significant selectivity of this process implies that UV-light played an important role in the prebiotic selection of the most photochemically stable nucleic acid sequences.[24]

Many fundamental aspects of the photochemistry of nucleic acid oligomers (such as GAT=T) are still obscure, including the relative contribution of locally-excited (LE) and delocalized excitations in DNA strands, the extent of the charge-transfer (CT) character of the latter, and the availability of different

[a]Institute of Physics, Polish Academy of Sciences, Al. Lotników 32/46, PL-02668 Warsaw, Poland

[b]Institute of Biophysics of the Czech Academy of Sciences, Královopolská 135, 61265 Brno, Czech Republic. E-mail: szabla@ibp.cz

[c]Regional Centre of Advanced Technologies and Materials, Department of Physical Chemistry, Faculty of Science, Palacký University, 17. Listopadu 1192/12, 77146 Olomouc, Czech Republic

photorelaxation pathways in such assemblies.[25,26] While some valuable insights into these processes were provided by time-resolved (TR) spectroscopic (*e.g.* transient absorption UV) techniques,[27] it is generally difficult to study the clear origin of the long-lived states due to overlapping absorption features of different nucleobases.[25] In addition, selective synthesis of specific photodamaged sequences is challenging. On the other hand, considerable system sizes often restrict the applications of theoretical simulations to methods such as Time-Dependent Density Functional Theory (TDDFT). Even though TDDFT was employed with some success in investigations of photochemical and photophysical properties of oligonucleotides,[28,29] the applicability of this methodology to similar problems has been criticized because of often significant overstabilization of CT states.[26,30,31] While range-separated functionals can alleviate this problem to some extent for vertical excitations, nonadiabatic molecular dynamics simulations of adenine with TDDFT failed to correctly describe the excited-state lifetimes and photo-deactivation pathways.[32]

In the light of the above discussion, characterization of photoinduced processes in oligonucleotides based on highly accurate quantum-chemical methods is urgently needed. In particular, a much more balanced description of the LE and CT states, even outside the Franck–Condon region, can be obtained with the algebraic diagrammatic construction to the second order [ADC(2)] method.[33,34] The ADC(2) method was recently proved to provide reliable results in the investigations of the photochemistry of nucleic acids fragments within the QM/MM framework (referred to as ADC(2)/MM from here on).[26,35–39] However, these simulations only involved the nucleobases treated at the ADC(2) level and the effects of the truncation of the QM region at the *N*-glycosidic bond are unclear. Moreover, previous studies did not consider optimizations of minimum-energy crossing points (MECPs) at the ADC(2)/MM level, which are crucial in understanding the reactivity of different electronic states participating in the photochemistry of oligonucleotides.

Our goal is to identify the possible mechanistic features and intermediate states that govern the sequence selective self-repair in nucleic acid fragments, first observed by Bucher *et al.*[23] For this purpose, we employ the ADC(2)/MM protocol (nucleobases treated at the ADC(2) level) to optimize the minimum-energy geometries and compare the relative energies of different LE and delocalized states in the GAT=T oligomer. We further discuss MECP optimizations and validate the energies of all stationary points by including the whole tetranucleotide in the QM region. This enables us to expose some of the potential pitfalls of the previous approaches, like often incorrect prediction of the relative energies of intermediate delocalized states. Based on these simulations we propose that the photochemical self-repair of the GAT=T sequence can be envisioned as a sequential electron transfer (SET) process which involves multiple changes of the orbital (diabatic) character of the S_1 state occurring downhill along the slope of the S_1 potential energy surface, after the local excitation of one of the purine bases.

Computational methods

MD simulations

The initial geometry of the GAT=T tetranucleotide was prepared in the B-DNA helical form. The T=T residue was prepared in the same way as the standard AMBER nucleotides.[40] The torsion parameters for the cyclobutane ring in the T=T dimer given by the standard atomic types of the parmOL15 force field[41–44] were found satisfactory according to our test simulation. MD simulations were carried out under the parmOL15 force field[41–44] in an octahedral box of explicit water molecules (either SPC/E,[45] or OPC model[46]) with 0.15 M excess KCl,[47] using the AMBER software package.[48] Each of these simulations was propagated for 10 μs. The trajectories were clustered by a custom modified algorithm[49] of Rodriguez *et al.*,[50] using the eRMSD metric.[51] More details about the MD simulations are included in the ESI† to this article.

QM/MM simulations

The geometries of selected (GA-*anti* and GA-*syn*) conformers obtained from the clustering procedure were further utilized in the QM/MM calculations. These geometries were solvated in a spherical droplet of SPC/E explicit water molecules, with a radius of 25 Å. The solvent was then equilibrated for 10 ps, in order to obtain a reasonable distribution of the water molecules within the sphere. We considered two different QM/MM setups: QM_{DNA}/MM setup contained the whole tetranucleotide treated at the QM level, while only the nucleobases were included in the QM region of QM_{bases}/MM setup (see Fig. 1, for the pictorial representation). In fact, QM_{bases}/MM setup is the primarily used setting in many calculations considering the photochemistry and photophysics of nucleic acid fragments.[52,53] The link hydrogen atom scheme was applied in QM_{bases}/MM setup, where the boundary between the QM and MM regions bisected the covalent *N*-glycosidic bonds. The point charge of the MM link hydrogen atom was set to zero, to avoid overpolarization.[54] These simulations were performed using a locally-modified
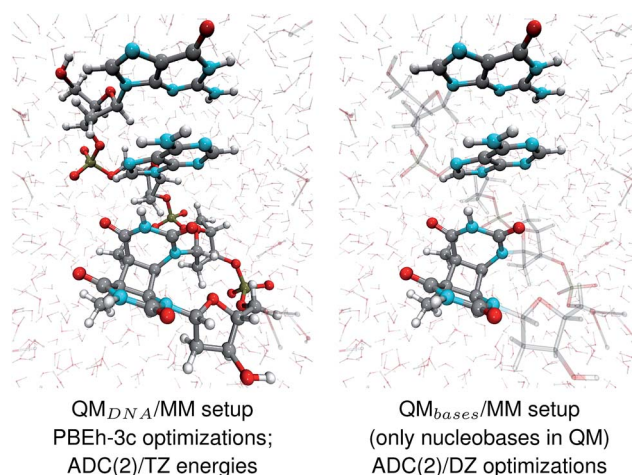

Fig. 1 The two QM/MM setups applied to the energy calculations and structural optimizations performed in this work.

QM/MM interface[54] of the AMBER suite of programs[48] to enable QM calculations employing the TURBOMOLE 7.1 program,[55] within the electrostatic embedding framework.

The QM/MM optimizations of the ground-state equilibrium geometries were first performed using QM_{DNA}/MM setup and the low-cost hybrid DFT composite scheme, PBEh-3c.[56] The PBEh-3c method was recently shown to be particularly well suited for calculations of RNA tetranucleotides.[57] The initial optimizations were performed for the whole QM/MM system using the internal AMBER[48] optimizer and the limited-memory BFGS method. These geometries were reoptimized with tighter convergence criteria using a rational function and approximate normal coordinates scheme as implemented in the open-source optimizer XOPT.[58–60] During the reoptimization procedure only the atom positions in an inner spherical region of the QM/MM system were relaxed, while the outer region was kept frozen. The inner region contained all the atoms within 11.5 Å of the most central atom of the GA-*anti* conformer and 12.5 Å of the most central atom of the GA-*syn* conformer. The inner region was in each case carefully selected to keep an appropriate solvation shell around the tetranucleotide. This approach was also applied in the excited-state calculations.

The algebraic diagrammatic construction to the second order [ADC(2)][33,34,61] method was used in all the excited-state calculations. The ADC(2) method was shown to yield a correct description of the excited-state potential energy surfaces of adenine and thymine outside the Franck–Condon region.[32,62] The vertical excitation energies and oscillator strengths were calculated on top of the PBEh-3c geometries, using the QM_{bases}/MM setup, ADC(2) method and the TZVP basis set. The QM_{bases}/MM setup was also used in the ADC(2)/MM optimizations of the different minima on the PE surface of the S_1 state and all the minimum-energy crossing points (MECPs). The TheoDORE 1.5.1 package was used to establish the charge transfer numbers and perform electron–hole population analysis.[63,64] The molecular orbitals were generated using the IboView program.[65] MECPs were optimized employing the approach of Levine, Coe and Martínez,[66] which was recently shown to provide reliable $S_1(\pi\pi^*)/S_0$ conical intersection geometries in several biomolecular systems without the evaluation of nonadiabatic couplings.[67,68] This scheme was included in the XOPT code to enable the optimization of state crossings within the QM/MM framework. Even though, it was indicated that the ADC(2)/MP2 methods may fail to correctly reproduce the topography of $n\pi^*/S_0$ state crossings in nucleobases,[68] all of the S_1/S_0 MECPs considered in this work involved $\pi\pi^*$ excitations, and consequently we anticipate the corresponding MECP geometries to be reliable. To keep consistent geometries when comparing the energies of different excited state minima with the Franck–Condon region, the ground-state geometry was additionally optimized using QM_{bases}/MM setup and MP2/MM approach. All of the ADC(2)/MM and MP2/MM optimizations were performed with the def2-SVP basis set. In addition, the energies of all the stationary points were recalculated using the QM_{DNA}/MM setup (whole tetranucleotide in the QM region) ADC(2) and MP2 methods and the larger TZVP basis set.

Results and discussion

MD simulations and conformational analysis

We performed Molecular Dynamics (MD) simulations of the GAT=T tetranucleotide to explore its conformational space and asses the population of different structural arrangements. Our main goal was to establish the availability of different fully stacked conformations, which could readily assist in the sequential electron transfer process responsible for the self-repair of CpD lesions, as described by Bucher *et al.*[23] Even though force-field based MD simulations of DNA and RNA tetramers frequently yield spurious populations of experimentally unconfirmed conformers,[69–71] better agreement with experiments was obtained for r(GACC) and r(CCCC) by employing more accurate solvent models, like OPC.[46,68,72] Consequently, we carried out 10 μs-long MD simulations employing one of the traditionally used 3-point water models SPC/E, and the conceivably more accurate 4-point water model OPC,[46] for comparison. Both the SPC/E and OPC simulations yielded qualitatively consistent populations of the fully stacked conformations of the GAT=T tetramer, *i.e.* 54.1% and 45.5% respectively. While some discrepancies between these two simulation runs are apparent, we focus on discussing the two conformers which could potentially have the largest contribution to the overall photochemistry either in the tetranucleotide or in longer DNA strands (*cf.* Fig. 2).

The majority of the ADC(2)/MM calculations were performed for the GA-*anti* conformer, which has the *anti* orientation of the G and A bases and represents the spatial arrangement of the GAT=T sequence in longer DNA strands. Since the population of the GA-*anti* conformer is relatively low (3.2% based on the OPC simulations), we additionally considered the GA-*syn* conformer having both the G and A bases in the *syn* orientation with respect to the sugar moieties. Both the SPC/E and OPC simulations indicate that the GA-*syn* conformer is the dominant molecular arrangement with the estimated populations of 47.0% and 31.2%, respectively. The ADC(2)/MM calculations
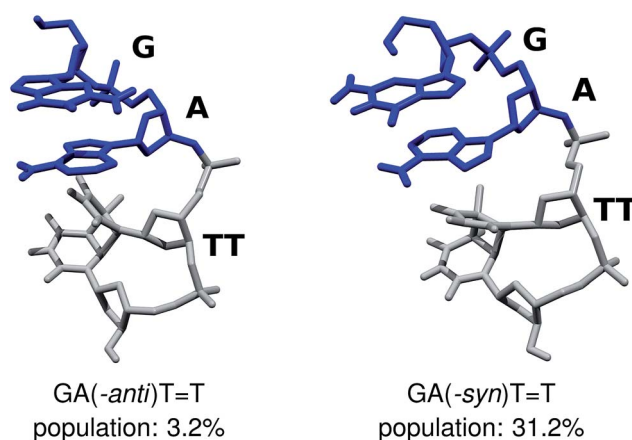

Fig. 2 The GA-*anti* and GA-*syn* conformers of the GAT=T tetranucleotide, considered in the ADC(2)/MM simulations. The populations shown above were extracted from MD simulations employing the OPC water model.

performed for the GA-*syn* are shown in the ESI,† since the major conclusions regarding the self-repair mechanism remained unchanged in both studied cases. We also identified two other conformers which contributed to the ensemble of fully stacked geometries, namely the G-*syn*-A-*anti* and G-*anti*-A-*syn* substates, but were not examined in the further ADC(2)/MM calculations.

Vertical excitation energies

The averaged OPC structures of the GA-*syn* and GA-*anti* conformers were further optimized using the QM_{DNA}/MM setup (Fig. 1) and the PBEh-3c method. Based on these geometries we calculated the vertical excitation energies using the QM_{bases}/MM setup and the ADC(2)/TZVP method (*cf.* Table 1 for the GA-*anti* conformer). As observed previously for other DNA oligomers,[26,38] the lower-energy range of the spectrum is populated by locally excited states, while the lowest-lying CT of the GA-*anti* conformer state can be classified as the S_{10} state and is associated with an electron transferred from the A purine base to the T=T dimer. The lower part of the spectrum is essentially dominated by $\pi\pi^*$ and $n\pi^*$ excitations localized on the respective bases.

The lowest-lying locally-excited $\pi_G\pi_G^*$ state on the G base has an excitation energy of 4.91 eV and is the lowest-energy excitation (S_1) in the whole tetranucleotide. We expect that this state was predominantly populated in the experiments conducted by Bucher *et al.*,[23] which involved photoexcitation in the UVB spectral range ($\lambda_{exc} = 290$ nm, 4.28 eV). The optically bright $\pi_A\pi_A^*$ transitions associated with the A base correspond to the S_3 and S_4 states in the GAT=T tetranucleotide and can be accessed at slightly higher excitation energies, *i.e.* 5.11 eV and 5.21 eV. The remaining states present in the lower energy range of the spectrum are $n\pi^*$ excitations localized on the C4=O groups of the T=T dimer. These $n\pi^*$ states were previously suggested to participate in the direct self-repair of the T=T dimers. However, the MM solvent is represented by a point charge scheme and many electronic effects crucial for the dark $n\pi^*$ are neglected in this approach. In fact, it was demonstrated that the inclusion of explicit QM water molecules results in considerable blue-shift of $n_O\pi^*$ states.[73,74] Here, the consideration of all the neighbouring water molecules at the QM level is beyond our computational capabilities, albeit we expect that such blue-shift of these $n_O\pi^*$ states in the GAT=T tetranucleotide would

significantly decrease their availability in the photochemical processes studied in this work. The $\pi\pi^*$ excitations associated with the T=T dimer can be also found in higher energy range of the spectrum.

Sequential electron transfer

Assuming the initial population of the $\pi_G\pi_G^*$ state, we expect all the subsequent photophysical and photochemical processes to occur on the S_1 hypersurface. The near proximity of several chromophores enables the formation of exciplex states and occurrence of charge transfer events resulting in changes of the character of the S_1 state. In fact, the multitude of possible excited-state phenomena makes the photochemistry of oligonucleotides much more complex when compared to isolated nucleobases. Here, we propose that the self-repair of the GAT=T tetramer can be envisioned as a sequential electron transfer involving consecutive changes of the diabatic character of the S_1 state. As shown in Fig. 3, each of the stationary points between the Franck–Condon region and the CpD ring-opening MECP corresponds to a local minimum associated with a different orbital character and the deduced mechanism operates downhill on the S_1 hypersurface.

Right after the photoexcitation, the GAT=T tetranucleotide can undergo vibrational relaxation to the minimum of the $\pi_G\pi_G^*$ state (denoted as G* in Fig. 3) associated with moderate puckering of the guanine base. This ring puckering effect is most pronounced at the C4 and C5 atoms in the GA-*anti* conformer and the C2 carbon atom connected to the amino group in the case of the GA-*syn* conformer. From these $\pi_G\pi_G^*$ minima the system can reach the $\pi\pi^*/S_0$ conical intersection described before as the dominant photodeactivation channel in isolated guanine.[75,76] This state crossing in the GA-*syn* conformer is characterized by a more pronounced puckering of the C2 carbon atom and a slightly sloped topography, since it lies 0.15 eV above the $\pi_G\pi_G^*$ minimum. Based on analogous calculations and virtually identical results for isolated guanine, we anticipate that the photorelaxation of UV-excited guanine in the GA-*syn* conformer resembles the photodeactivation mechanisms reported in gas phase studies.[75] In contrast, our optimizations of the $\pi_G\pi_G^*/S_0$ MECP in the GA-*anti* conformer yielded a C4-puckered geometry that lies 0.5 eV above the respective $\pi_G\pi_G^*$ minimum. This suggests that some of the monomeric photodeactivation channels in oligonucleotides may be significantly hindered in selected conformers due to the interactions with neighbouring bases.

Alternatively, the GAT=T tetranucleotide containing UV-excited guanine may follow a relaxation pathway on the S_1 surface towards a further local minimum possibly associated with a CT or exciplex state. This scenario was previously hypothesized by Bucher *et al.*,[23] who suggested that the $G^{+\bullet}A^{-\bullet}$ state could be the key intermediate state that precedes the electron transfer to the T=T dimer.[23] Our ADC(2)/MM calculations reveal that even though the $G^{+\bullet}A^{-\bullet}$ ($\pi_G\pi_A^*$) state lies above the S_{10} state in the Franck–Condon region of the GA-*anti* conformer, it is significantly red-shifted during the initial vibrational relaxation of the UV-excited guanine. In fact both the

Table 1 Vertical excitation energies (in eV) of the GA(-*anti*) conformer, computed assuming the QM_{bases}/MM setup at the ADC(2)/TZVP level based on the PBEh-3c/MM ground-state geometry

GA(-*anti*)T=T conformer

State/transition		E_{exc}/[eV]	f_{osc}	λ/[nm]
S_1(LE)	$\pi_G\pi_G^*$	4.91	8.06×10^{-2}	252.5
S_2(LE)	$n_{TT}\pi_{TT}^*$	4.94	1.40×10^{-3}	251.0
S_3(LE)	$\pi_A\pi_A^*$	5.11	19.8×10^{-2}	242.6
S_4(LE)	$\pi_A\pi_A^*$	5.21	6.40×10^{-2}	238.0
S_5(LE)	$n_{TT}\pi_{TT}^*$	5.26	6.40×10^{-2}	235.7
S_{10}(CT)	$\pi_A\pi_{TT}^*$	5.81	7.38×10^{-3}	213.4

Fig. 3 Sequential electron transfer (SET) mechanism initiated in the $\pi_G \pi_G^*$ LE state involves several changes of the diabatic character of the S_1 state. These changes can be associated with the existence of different local minima available downhill along the slope of the S_1 PE surface. The geometry optimizations were performed using QM$_{bases}$/MM setup and the ADC(2)/def2-SVP method, while the energies shown above were obtained using the QM$_{DNA}$/MM setup and the ADC(2)/TZVP method.

S_2 and S_3 excitations, computed on the $\pi_G \pi_G^*$ LE minimum-energy geometry, are delocalized states involving charge transfer between the G and A bases. In particular, the $G^{+\cdot}A^{-\cdot}$ state considered by Bucher et al.,[23] lies merely 1.59 eV above the $\pi_G \pi_G^*$ LE minimum and corresponds to the S_3 state. Surprisingly, the S_2 state lying 1.26 eV above the $\pi_G \pi_G^*$ LE minimum is characterized by an opposite electron transfer from adenine to guanine. While we successfully optimized the S_1 minimum corresponding to the $G^{+\cdot}A^{-\cdot}$ state, we could not locate the $G^{-\cdot}A^{+\cdot}$ minimum at the ADC(2)/MM level and we anticipate that this latter state is not involved in the photoreactivity of the GAT=T tetramer.

The $G^{+\cdot}A^{-\cdot}$ minimum lies 0.9 eV below the $\pi_G \pi_G^*$ LE minimum and may become the direct precursor of the $\pi_G \pi_{TT}^*$ CT state which entails an electron transfer to the T=T dimer. In other words, the negatively charged adenine could readily transfer its excess electron to the T=T dimer leading to the formation of the reactive state with self-repair propensity. This $G^{+\cdot}AT=T^{-\cdot}$ minimum is again lower in energy than the preceding stationary point, by nearly 0.5 eV. In addition, we located another local minimum on the S_1 surface containing the negatively charged CpD, namely the $GA^{+\cdot}T=T^{-\cdot}$ ($\pi_A \pi_{TT}^*$) state. The ADC(2)/MM energies computed for the whole tetranucleotide reveal that the latter CT minimum having the positive charge localized on the A base is, in fact, the lowest-energy S_1 minimum available in the GA-syn conformer and possibly the last link in the SET mechanism before the actual T=T dimer repair.

Our optimizations of the S_1/S_0 MECP initiated from both the $GA^{+\cdot}T=T^{-\cdot}$ and $G^{+\cdot}AT=T^{-\cdot}$ minimum-energy geometries converged to the same $\pi_A \pi_{TT}^*/S_0$ state crossing. This MECP is characterized by a partially opened cyclobutane ring with the C5–C5 bond being broken and the C6–C6 bond remaining the single covalent connection between the two thymine bases (cf. Fig. 3). We anticipate that this self-repair mechanism can operate from both the $GA^{+\cdot}T=T^{-\cdot}$ and $G^{+\cdot}AT=T^{-\cdot}$ minima, since the primary factor that enables the T=T dimer repair is the electron transfer to the photolesion and not the location of the hole (positive charge) in the system.

It is generally difficult to envisage the exact reaction coordinates leading to the transitions between the different stationary points presented in Fig. 3, owing to the large number of nuclear degrees of freedom in the GAT=T tetramer. In other words, S_1 hypersufaces of oligonucleotides are significantly more complex when compared to isolated nucleosides and nucleobases. However, we anticipate that the local minima constituting the SET mechanism are rather shallow and we expect the energy barriers separating the consecutive stages to be generally low. This is reflected by the high sensitivity of the excited-state optimizations to the initial guess geometry, i.e. sometimes small changes in the initial geometry may result in convergence to another local minimum on the S_1 hypersurface. Another important factor which determines the efficiency of the transitions between the different minima is the availability of S_1/S_0 conical intersections from the intermediate states. As we have shown above, the high energy of the $\pi_G \pi_G^*/S_0$ state

crossing will facilitate the population of the $G^{+\cdot}A^{-\cdot}$ minimum. Limited accessibility of the $\pi_G\pi_A^*/S_0$ state crossings is discussed below. As pointed out by Lee and co-workers,[16] the evaluation of diabatic coupling matrix elements (DCMEs) between the electronic states is crucial for proving the validity of a proposed photoreaction mechanism. Our estimates based on the generalized Mulliken Hush and Boys localization approaches,[77,78] yielded DCMEs exceeding 0.1 eV between the consecutive electronic states. This implies that the electron transfer events in the GAT=T could be indeed very efficient. Nevertheless, our DCME estimates require a separate commentary, which can be found in the ESI.† A detailed and accurate description of the transition paths between the different stationary points in the SET mechanism could be inferred from nonadiabatic molecular dynamics simulations, but this approach is currently beyond our computational capabilities for systems of this size.

The characteristics of the available intermediate states

Intermediate states with charge transfer character play a central role in driving the GAT=T tetramer towards the S_1/S_0 conical intersection responsible for C5–C5 bond breaking of the CpD lesion. Therefore, understanding their most distinctive features is essential in finding the photoreaction pathway responsible for the self-repair of a given oligonucleotide. The molecular orbitals associated with each of the proposed intermediate states in the GA-*anti* conformer are presented in Fig. 4. The dominant π (occupied; blue and violet) and π^* (virtual; green and yellow) molecular orbitals contributing in at least 88% to each of these excitations clearly demonstrate their CT character.

Apart from the three CT states already mentioned in the SET mechanism, we also located one exciplex state shared between the G and A bases which does not have any notable CT character. The corresponding geometry of the GA-exciplex minimum is presented in the top left panel of Fig. 4. The ADC(2) optimizations performed using the QM_{bases}/MM setup initially indicated that the GA-exciplex state could be the first intermediate reached from the $\pi_G\pi_G^*$ LE state. At the same time, the ADC(2) energy of the $G^{+\cdot}A^{-\cdot}$ minimum obtained using the QM_{bases}/MM setup was higher than the $\pi_G\pi_G^*$ LE minimum. However, this picture is completely different when the ADC(2) energies are recalculated within the QM_{DNA}/MM setup, *i.e.* when the sugar-phosphate backbone is included in the QM region. We presume that this unexpected behavior is the result of strong differences in the electric dipole moment direction and magnitude between the QM_{DNA}/MM and QM_{bases}/MM setups characteristic for these two particular states. In other words, the QM_{bases}/MM setup is incapable of correctly reproducing the μ vectors of the $G^{+\cdot}A^{-\cdot}$ and GA-exciplex states, which substantially affects the relative energies of the states in the field of electrostatic point charges. The relative energies of the remaining intermediate states are not affected by the size of QM region in the qualitative sense. Nevertheless, the example of the GA-exciplex and $G^{+\cdot}A^{-\cdot}$ intermediate states shows that the truncation of the QM region at the *N*-glycosidic bond might result in deceptive results and considerable care needs to be taken
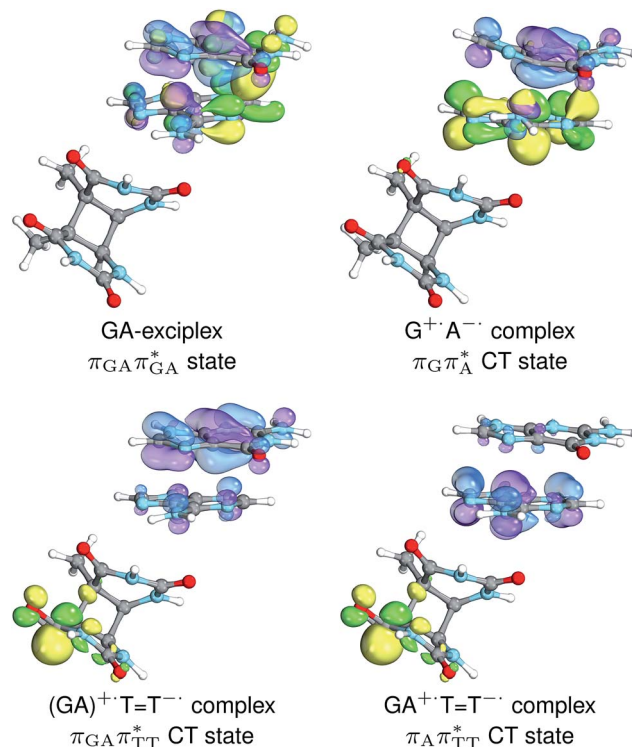

Fig. 4 Occupied (transparent blue and violet) and virtual (solid green and yellow) molecular orbitals associated with the selected delocalized states found for the GA-*anti* conformer of the GAT=T tetramer (molecular orbital weight >88%). In the case of CT states, the occupied and virtual orbitals present the approximate location of the hole and the transferred electron, respectively.

during the prediction of relative energies of different electronic states in nucleic acids within the QM/MM framework.

The electron–hole population analysis shows that the $G^{+\cdot}A^{-\cdot}$ state is associated with 0.57 and 0.45 electron transferred from guanine to adenine in the corresponding $G^{+\cdot}A^{-\cdot}$ S_1 minima of the GA-*anti* and GA-*anti* conformers. The consecutive $\pi_G\pi_{TT}^*$ CT state accessed in the GA-*anti* conformer involves a transfer of $0.97\ e^-$ to the T=T dimer from the G and A bases, where $0.55\ e^-$ is transferred from G and $0.42\ e^-$ from A. In contrast, the corresponding $\pi_G\pi_{TT}^*$ CT state found in the GA-*syn* conformer involves a transfer of $0.94\ e^-$ to the T=T dimer occurring exclusively from the G base. However, we denote this state as $G^{+\cdot}AT=T^{-\cdot}$, to keep a uniform naming scheme for both studied conformers. Finally, the $GA^{+\cdot}T=T^{-\cdot}$ minimum in the GA-*anti* conformer is associated with $0.96\ e^-$ transferred to the T=T dimer, where the majority of the hole (0.87) is located on the A base. These results confirm the previous suggestion that CT states could involve delocalization of the transferred charge over the neighbouring bases.[25] However, we expect this feature to be dependent on the local arrangement of nucleobases, since it is present in only one of the studied conformers.

The charge transfer process occurring from guanine to adenine results in the formation of fascinating interactions between the two bases (*cf.* Fig. 5). In the case of the GA-*anti* conformer, a strong interaction is created between the C5 atom of guanine and the amino group of adenine associated with
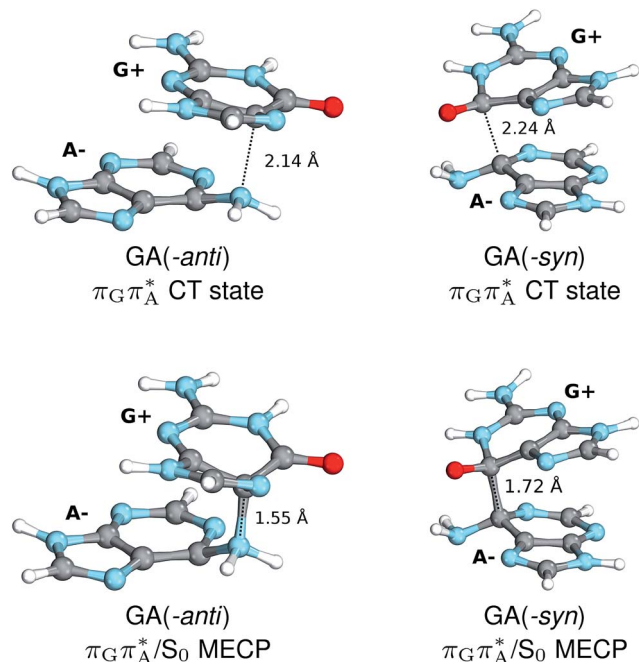
Fig. 5 Geometries of the different $G^{+\bullet}A^{-\bullet}$ S_1 minima located for both GA-*syn* and -*anti* conformers (top), and the corresponding S_1/S_0 MECPs (bottom). The optimizations were performed using QM$_{bases}$/MM setup, but only the G and A bases are shown for clarity.

a C5···NH$_2$ distance of 2.14 Å. On the contrary, the $G^{+\bullet}A^{-\bullet}$ state in the GA-*syn* conformer leads to the formation of an interaction between the C6 atom of guanine and the C6 atom of adenine with the equilibrium distance of 2.24 Å. Shortening of these two distances leads to $\pi_G\pi_A^*/S_0$ conical intersections and covalent bond formation between the two bases. The optimized $\pi_G\pi_A^*/S_0$ MECP lies 0.25 eV below the $G^{+\bullet}A^{-\bullet}$ minimum in the GA-*anti* conformer and these two points on the PES are separated by a modest energy barrier of ∼0.1 eV. Interestingly, the $\pi_G\pi_A^*/S_0$ MECP located in the GA-*syn* conformer lies 0.42 eV above the corresponding local minimum, which indicates that this state crossing is much less available and the corresponding $\pi_G\pi_A^*$ state is presumably long-lived, at least in this particular arrangement of the G and A bases. Indeed, Bucher *et al.* observed the existence of a charge-separated intermediate state with a lifetime of ∼300 ps, which is in excellent agreement with our picture.

CpD ring opening and T=T dimer repair

As we have already pointed out, the CpD ring opening is initiated in one of the CT states where the negative charge is located on the T=T dimer. According to our calculations, the opening of the C5–C5 bond between the two thymine bases is the first step during the actual CpD ring cleavage, and the $GA^{+\bullet}T=T^{-\bullet}$ minimum with closed CpD ring is very shallow. The relaxed scan in Fig. 6 demonstrates that stretching of the C5–C5 bond by merely 0.1 Å out of the equilibrium arrangement leads to the region of the PES where the partial CpD ring opening process occurs spontaneously. The C5···C5 distance at the $\pi_A\pi_{TT}^*/S_0$
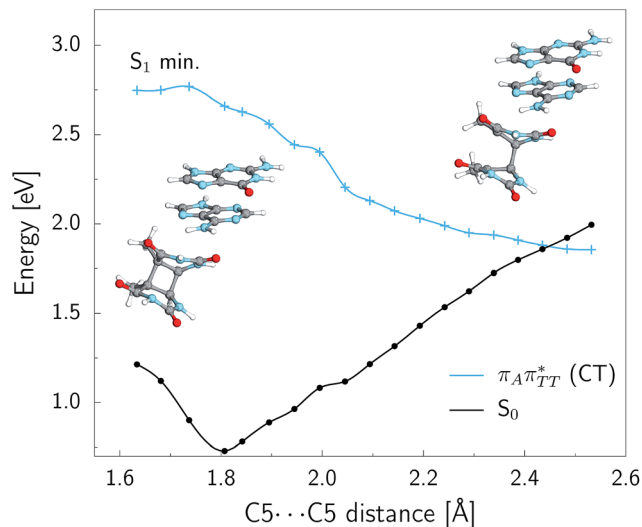

Fig. 6 Potential energy profile presenting the T=T CpD ring opening occurring on the surface of the $GA^+T=T^-$ state. The geometries along the profile were obtained by performing a relaxed scan along the C5···C5 distance using the QM$_{bases}$/MM setup. The energies presented above were extracted from single-point calculations using the QM$_{DNA}$/MM setup and the ADC(2)/TZVP method.

MECP amounts to 2.54 Å, while the C6–C6 bond length amounts to 1.58 Å and is nearly not affected at this stage. The peaked topography of this state crossing visible in Fig. 6 suggests that this crucial phase of the self-repair process efficiently drives the oligonucleotide to the electronic ground state with partially regenerated thymine bases.

The T=T dimer repair process can be eventually completed by C6–C6 bond cleavage in the vibrationally hot electronic ground state of the tetranucleotide, *i.e.* after the photo-relaxation through the $\pi_A\pi_{TT}^*/S_0$ conical intersection. Such sequential and nearly barrierless CpD ring opening initiated at the C5–C5 site was also proposed based on DFT/MM simulations of the T=T dimer in the radical-anionic form.[79] The optimization of the ground state geometry starting from the $\pi_A\pi_{TT}^*/S_0$ MECP shows that C6–C6 bond rupture occurs in a barrierless manner when at least weak restraints are imposed on the C5···C5 distance to prevent its closure. If no restraints are imposed, the C5–C5 bond is spontaneously reformed and the CpD structure can be recovered. Such bifurcation after passing through a S_1/S_0 conical intersection is typical for many fundamental photochemical reactions, and we anticipate that the dynamic system can yield either the repaired thymine bases or the CpD depending on the momentary arrangement of the surroundings when the discussed state crossing is reached. It is worth to note, that this stepwise mechanism was recently proposed to govern the UV-induced formation of T=T dimers in the triplet manifold, which is the opposite reaction to the self-repair process described in this work.[17]

Conclusions

Based on the ADC(2)/MM calculations we propose that the self-repair of the CpD lesion in the GAT=T tetramer can be

rationalized in terms of the sequential electron transfer (SET) mechanism. This process is initiated in one of the optically bright LE states of the tetranucleotide (*e.g.* $\pi_G\pi_G^*$ state) and is associated with consecutive electron transfer processes and changes of the orbital character occurring downhill in energy on the S_1 hypersurface. The CpD repair process may be triggered in one of the lowest-lying S_1 minima containing an excessive electron located on the T=T dimer (either $G^{+\cdot}AT=T^{-\cdot}$ or $GA^{+\cdot}T=T^{-\cdot}$). The CpD ring opening is then preferentially started at the C5–C5 site and leads to the S_1/S_0 conical intersection with virtually no barrier. The self-repair process is eventually completed by the C6–C6 bond rupture in the vibrationally hot ground state of the tetranucleotide.

The MECP optimizations enabled us to assign the long-lived state observed by Bucher *et al.*, to the $\pi_G\pi_A^*$ CT state ($G^{+\cdot}A^{-\cdot}$) in the GA-*syn* conformer. The experimental lifetime of 300 ps is clearly reflected by the presence of the sloped $\pi_G\pi_A^*/S_0$ MECP which lies 0.42 eV above the $G^{+\cdot}A^{-\cdot}$ minimum.

The qualitative features of the SET mechanisms are conserved in both studied conformers, but some specific differences are evident. For instance, the stacking pattern strongly differs in the *syn/anti* conformers, while retaining the same (formal) intermediate $\pi_G\pi_A^*$ state (*cf.* the $G^{+\cdot}A^{-\cdot}$ minima in Fig. 5). The different interaction mode from the stacking variants leads to a significantly different energies of the S_1/S_0 state crossings in the $G^{+\cdot}A^{-\cdot}$ intermediate, resulting in different lifetimes and presumably conformer-dependent self-repair efficiency. This suggests that a more complete understanding of the photochemistry of short oligonucleotides requires conformational sampling.

We propose the main criteria which could help in identifying these nucleic-acid sequences which could efficiently promote self-repair of CpD lesions:

(i) The CT states containing the excess electron residing on the CpD lesion should be available directly or indirectly from the LE states populated soon after the photoexcitation.

(ii) The CpD repairing state can be accessed indirectly *via* several local S_1 minima corresponding to intermediate diabatic states, within the SET mechanism. An efficient SET mechanism operates downhill along the S_1 hypersurface, the consecutive diabatic states should be strongly coupled and the local minima should be separated by rather low energy barriers.

(iii) The intermediate diabatic states should have sufficiently long excited-state lifetimes to prevent premature relaxation to the S_0 state and enable efficient population of successive minima in the SET mechanism. This property can be deduced from the availability of S_1/S_0 conical intersections in the respective local S_1 minima.

Such predictive capacity is critical for deciphering the yet unclear stages of abiogenesis, since the emergence of first oligonucleotides on our planet was presumably regulated by high UV fluxes and the lack of photolesion repair factors.

Conflicts of interest

There are no conflicts to declare.

References

1 J. S. Taylor, *Acc. Chem. Res.*, 1994, **27**, 76–82.
2 R. P. Sinha and D.-P. Häder, *Photochem. Photobiol. Sci.*, 2002, **1**, 225–236.
3 S. Weber, *Biochim. Biophys. Acta, Bioenerg.*, 2005, **1707**, 1–23.
4 T. Todo, H. Takemori, H. Ryo, M. Lhara, T. Matsunaga, O. Nikaido, K. Sato and T. Nomura, *Nature*, 1993, **361**, 371–374.
5 J. E. Cleaver and E. Crowley, *Front. Biosci.*, 2002, 7, d1024–1043.
6 B. A. Gilchrest, M. S. Eller, A. C. Geller and M. Yaar, *N. Engl. J. Med.*, 1999, **340**, 1341–1348.
7 J. T. Reardon and A. Sancar, *Genes Dev.*, 2003, **17**, 2539–2551.
8 S. Faraji, D. Zhong and A. Dreuw, *Angew. Chem., Int. Ed.*, 2016, **55**, 5175–5178.
9 S. Faraji and A. Dreuw, *Photochem. Photobiol.*, 2017, **93**, 37–50.
10 S. Faraji and A. Dreuw, *Annu. Rev. Phys. Chem.*, 2014, **65**, 275–292.
11 W. J. Schreier, T. E. Schrader, F. O. Koller, P. Gilch, C. E. Crespo-Hernández, V. N. Swaminathan, T. Carell, W. Zinth and B. Kohler, *Science*, 2007, **315**, 625–629.
12 L. Liu, B. M. Pilles, J. Gontcharov, D. B. Bucher and W. Zinth, *J. Phys. Chem. B*, 2016, **120**, 292–298.
13 C. Rauer, J. J. Nogueira, P. Marquetand and L. González, *J. Am. Chem. Soc.*, 2016, **138**, 15911–15916.
14 W. J. Schreier, J. Kubon, N. Regner, K. Haiser, T. E. Schrader, W. Zinth, P. Clivio and P. Gilch, *J. Am. Chem. Soc.*, 2009, **131**, 5038–5039.
15 K. Haiser, B. P. Fingerhut, K. Heil, A. Glas, T. T. Herzog, B. M. Pilles, W. J. Schreier, W. Zinth, R. de Vivie-Riedle and T. Carell, *Angew. Chem., Int. Ed.*, 2012, **51**, 408–411.
16 W. Lee, G. Kodali, R. J. Stanley and S. Matsika, *Chem.–Eur. J.*, 2016, **22**, 11371–11381.
17 C. Rauer, J. J. Nogueira, P. Marquetand and L. González, *Monatsh. Chem.*, 2018, **149**, 1–9.
18 S. Ranjan and D. D. Sasselov, *Astrobiology*, 2016, **16**, 68–88.
19 S. Ranjan and D. D. Sasselov, *Astrobiology*, 2017, **17**, 169–204.
20 C. S. Cockell and G. Horneck, *Photochem. Photobiol.*, 2001, **73**, 447–451.
21 C. S. Cockell, *Origins Life Evol. Biospheres*, 2000, **30**, 467–500.
22 R. J. Rapf and V. Vaida, *Phys. Chem. Chem. Phys.*, 2016, **18**, 20067–20084.
23 D. B. Bucher, C. L. Kufner, A. Schlueter, T. Carell and W. Zinth, *J. Am. Chem. Soc.*, 2016, **138**, 186–190.
24 A. A. Beckstead, Y. Zhang, M. S. d. Vries and B. Kohler, *Phys. Chem. Chem. Phys.*, 2016, **18**, 24228–24238.

25 D. B. Bucher, B. M. Pilles, T. Carell and W. Zinth, *Proc. Natl. Acad. Sci. U. S. A.*, 2014, **111**, 4369–4374.

26 V. A. Spata and S. Matsika, *Phys. Chem. Chem. Phys.*, 2015, **17**, 31073–31083.

27 C. T. Middleton, K. d. L. Harpe, C. Su, Y. K. Law, C. E. Crespo-Hernández and B. Kohler, *Annu. Rev. Phys. Chem.*, 2009, **60**, 217–239.

28 Y. Zhang, J. Dood, A. A. Beckstead, X.-B. Li, K. V. Nguyen, C. J. Burrows, R. Improta and B. Kohler, *Proc. Natl. Acad. Sci. U. S. A.*, 2014, **111**, 11612–11617.

29 L. Martinez-Fernandez, Y. Zhang, K. d. L. Harpe, A. A. Beckstead, B. Kohler and R. Improta, *Phys. Chem. Chem. Phys.*, 2016, **18**, 21241–21245.

30 A. Dreuw and M. Head-Gordon, *J. Am. Chem. Soc.*, 2004, **126**, 4007–4016.

31 N. T. Maitra, *J. Phys.: Condens. Matter*, 2017, **29**, 423001.

32 F. Plasser, R. Crespo-Otero, M. Pederzoli, J. Pittner, H. Lischka and M. Barbatti, *J. Chem. Theory Comput.*, 2014, **10**, 1395–1405.

33 A. B. Trofimov and J. Schirmer, *J. Phys. B: At., Mol. Opt. Phys.*, 1995, **28**, 2299.

34 A. Dreuw and M. Wormit, *Wiley Interdiscip. Rev.: Comput. Mol. Sci.*, 2015, **5**, 82–95.

35 V. A. Spata and S. Matsika, *J. Phys. Chem. A*, 2014, **118**, 12021–12030.

36 V. A. Spata, W. Lee and S. Matsika, *J. Phys. Chem. Lett.*, 2016, **7**, 976–984.

37 W. Lee and S. Matsika, *Phys. Chem. Chem. Phys.*, 2015, **17**, 9927–9935.

38 F. Plasser, A. J. A. Aquino, W. L. Hase and H. Lischka, *J. Phys. Chem. A*, 2012, **116**, 11151–11160.

39 F. Plasser and H. Lischka, *Photochem. Photobiol. Sci.*, 2013, **12**, 1440–1452.

40 W. D. Cornell, P. Cieplak, C. I. Bayly, I. R. Gould, K. M. Merz, D. M. Ferguson, D. C. Spellmeyer, T. Fox, J. W. Caldwell and P. A. Kollman, *J. Am. Chem. Soc.*, 1995, **117**, 5179–5197.

41 A. Pérez, I. Marchán, D. Svozil, J. Sponer, T. E. I. Cheatham, C. A. Laughton and M. Orozco, *Biophys. J.*, 2007, **92**, 3817–3829.

42 M. Krepl, M. Zgarbová, P. Stadlbauer, M. Otyepka, P. Banáš, J. Koča, T. E. Cheatham, P. Jurečka and J. Šponer, *J. Chem. Theory Comput.*, 2012, **8**, 2506–2520.

43 M. Zgarbová, F. J. Luque, J. Šponer, T. E. Cheatham, M. Otyepka and P. Jurečka, *J. Chem. Theory Comput.*, 2013, **9**, 2339–2354.

44 M. Zgarbová, J. Šponer, M. Otyepka, T. E. Cheatham, R. Galindo-Murillo and P. Jurečka, *J. Chem. Theory Comput.*, 2015, **11**, 5723–5736.

45 H. J. C. Berendsen, J. R. Grigera and T. P. Straatsma, *J. Phys. Chem.*, 1987, **91**, 6269–6271.

46 S. Izadi, R. Anandakrishnan and A. V. Onufriev, *J. Phys. Chem. Lett.*, 2014, **5**, 3863–3871.

47 I. S. Joung and T. E. Cheatham, *J. Phys. Chem. B*, 2008, **112**, 9020–9041.

48 D. Case, J. Berryman, R. Betz, D. Cerutti, T. Cheatham III, T. Darden, R. Duke, T. Giese, H. Gohlke, A. Goetz, N. Homeyer, S. Izadi, P. Janowski, J. Kaus, A. Kovalenko, T. Lee, S. Legrand, P. Li, T. Luchko, R. Luo, B. Madej, K. Merz, G. Monard, P. Needham, H. Nguyen, H. Nguyen, I. Omelyan, A. Onufriev, D. Roe, A. Roitberg, R. Salomon-Ferrer, C. Simmerling, W. Smith, J. Swails, R. Walker, J. Wang, R. Wolf, X. Wu, D. York and P. Kollman, *AMBER 14*, 2015.

49 P. Kührová, R. B. Best, S. Bottaro, G. Bussi, J. Šponer, M. Otyepka and P. Banáš, *J. Chem. Theory Comput.*, 2016, **12**, 4534–4548.

50 A. Rodriguez and A. Laio, *Science*, 2014, **344**, 1492–1496.

51 S. Bottaro, F. DiPalma and G. Bussi, *Nucleic Acids Res.*, 2014, **42**, 13306–13314.

52 R. Improta, F. Santoro and L. Blancafort, *Chem. Rev.*, 2016, **116**, 3540–3593.

53 J. J. Nogueira, F. Plasser and L. González, *Chem. Sci.*, 2017, **8**, 5682–5691.

54 A. W. Götz, M. A. Clark and R. C. Walker, *J. Comput. Chem.*, 2014, **35**, 95–108.

55 R. Ahlrichs, M. Bär, M. Häser, H. Horn and C. Kölmel, *Chem. Phys. Lett.*, 1989, **162**, 165–169.

56 S. Grimme, J. G. Brandenburg, C. Bannwarth and A. Hansen, *J. Chem. Phys.*, 2015, **143**, 054107.

57 R. Szabla, M. Havrila, H. Kruse and J. Šponer, *J. Phys. Chem. B*, 2016, **120**, 10635–10648.

58 H. Kruse, *local development version*, Institute of Biophysics, 2016, Brno, https://github.com/hokru/xopt.

59 H. Kruse and J. Šponer, *Phys. Chem. Chem. Phys.*, 2015, **17**, 1399–1410.

60 F. Eckert, P. Pulay and H.-J. Werner, *J. Comput. Chem.*, 1997, **18**, 1473–1483.

61 C. Hättig, *Advances in Quantum Chemistry*, Academic Press, 2005, vol. 50, pp. 37–60.

62 L. Stojanović, S. Bai, J. Nagesh, A. F. Izmaylov, R. Crespo-Otero, H. Lischka and M. Barbatti, *Molecules*, 2016, **21**, 1603.

63 F. Plasser, M. Wormit and A. Dreuw, *J. Chem. Phys.*, 2014, **141**, 024106.

64 F. Plasser, S. A. Bäppler, M. Wormit and A. Dreuw, *J. Chem. Phys.*, 2014, **141**, 024107.

65 G. Knizia, *J. Chem. Theory Comput.*, 2013, **9**, 4834–4843.

66 B. G. Levine, J. D. Coe and T. J. Martínez, *J. Phys. Chem. B*, 2008, **112**, 405–413.

67 D. Tuna, D. Lefrancois, Ł. Wolański, S. Gozem, I. Schapiro, T. Andruniów, A. Dreuw and M. Olivucci, *J. Chem. Theory Comput.*, 2015, **11**, 5758–5781.

68 R. Szabla, R. W. Góra and J. Šponer, *Phys. Chem. Chem. Phys.*, 2016, **18**, 20208–20218.

69 C. Bergonzo, N. M. Henriksen, D. R. Roe, J. M. Swails, A. E. Roitberg and T. E. Cheatham, *J. Chem. Theory Comput.*, 2014, **10**, 492–499.

70 J. D. Tubbs, D. E. Condon, S. D. Kennedy, M. Hauser, P. C. Bevilacqua and D. H. Turner, *Biochemistry*, 2013, **52**, 996–1010.

71 M. V. Schrodt, C. T. Andrews and A. H. Elcock, *J. Chem. Theory Comput.*, 2015, **11**, 5906–5917.

72 C. Bergonzo and T. E. Cheatham, *J. Chem. Theory Comput.*, 2015, **11**, 3969–3972.

73 N. A. Besley and J. D. Hirst, *J. Am. Chem. Soc.*, 1999, **121**, 8559–8566.

74 R. Szabla, H. Kruse, J. Sponer and R. W. Gora, *Phys. Chem. Chem. Phys.*, 2017, **19**, 17531–17537.

75 M. Barbatti, A. J. A. Aquino, J. J. Szymczak, D. Nachtigallová, P. Hobza and H. Lischka, *Proc. Natl. Acad. Sci. U. S. A.*, 2010, **107**, 21453–21458.

76 S. Yamazaki, W. Domcke and A. L. Sobolewski, *J. Phys. Chem. A*, 2008, **112**, 11965–11968.

77 R. J. Cave and M. D. Newton, *J. Chem. Phys.*, 1997, **106**, 9213–9226.

78 J. E. Subotnik, S. Yeganeh, R. J. Cave and M. A. Ratner, *J. Chem. Phys.*, 2008, **129**, 244101.

79 F. Masson, T. Laino, I. Tavernelli, U. Rothlisberger and J. Hutter, *J. Am. Chem. Soc.*, 2008, **130**, 3443–3450.